Journal of Microscopy, Vol. 226, Pt 1 April 2007, pp. 18–25
Received 17 August 2006; accepted 28 November 2006

Time-resolved fluorescence microscopy of gunshot residue: an application to forensic science

DAMIAN K. BIRD*, KENT M. AGG†, NEIL W. BARNETT† & TREVOR A. SMITH*
**Ultrafast and Microspectroscopy Laboratories, School of Chemistry, The University of Melbourne, Parkville, Victoria 3010, Australia*
†School of Life and Environmental Sciences, Deakin University, Geelong, Victoria 3217, Australia

Key words. Fluorescence microscopy, Forensic science, time resolved imaging, Confocal microscopy.

Summary

Time-resolved fluorescence microscopy has rapidly emerged as the technique of choice for many researchers aiming to gain specific insights into the dynamics of intricate biological systems. Although the unique advantages the technique provides over other methods have proven to be particularly useful in the biosciences, to date they have been largely unexploited by other research disciplines. In this paper, we demonstrate the capacity of time-resolved fluorescence microscopy as a practical analytical tool in the forensic sciences via the imaging of gunshot residues that are expelled when a firearm is discharged. This information may prove to be useful for determination of the true sequence of events that took place in a firearm related crime.

1. Introduction

Among the many fluorescence-based imaging techniques available to the research microscopist, time-resolved fluorescence microscopy [TRFM; or fluorescence lifetime imaging (FLIM)] is arguably the most powerful modality available to study biological function. This is largely due to the fact that (unlike conventional intensity based imaging approaches) the excited-state lifetime of a fluorophore is usually independent of its concentration and somewhat immune to attenuation by re-absorption and/or light scattering (Wang *et al.*, 1992). However, it is the extreme sensitivity of the excited-state lifetime of a fluorescent molecule to changes in the local microenvironment that makes it of particular interest; and it is this feature that enables the TRFM technique to provide valuable insights into specific molecular processes occurring within various components of the cell (Dickinson *et al.*, 2003).

Correspondence to: Damian K. Bird. Tel. +61 3 8344 6484; fax +61 3 9347 5180; e-mail: dbird@unimelb.edu.au

As a consequence, numerous studies have been reported in recent years that have utilized FLIM to monitor diverse parameters including pH, molecular association, oxygen concentration, Ca^{2+} concentration and proteolysis processing (Lakowicz, 1999; Periasamy, 2001). FLIM has also proven to be particularly useful as a diagnostic tool, finding scope in a diverse range of studies including oncological applications (Wagnieres *et al.*, 1998), histopathology (Eliceiri *et al.*, 2003), imaging of tissue constituents (Dowling *et al.*, 1998), studies of human skin (Cubeddu *et al.*, 1999; Becker *et al.*, 2002), cell cultures (Bastiaens and Squire, 1999), metabolic mapping of human breast cells (Bird *et al.*, 2005) and surveying inorganic contaminants present on the marble surface of the Statue of David (Toniolo *et al.*, 2004).

It is interesting to note, however, that although the unique advantages FLIM has to offer are proving to be particularly useful in the biosciences, to date they have been largely unexploited by other research disciplines. Considering the composition and structure of a range of samples that may inherently contain (or can be tagged with) fluorescent probes and be considered to be of a forensic nature, one exciting and rather intuitive application of FLIM is to the forensic sciences. Indeed, a handful of such studies have been reported, including nanosecond time-resolved spectroscopy of petroleum accelerants for solving crimes of arson (Saitoh and Takeuchi, 2005) and a feasibility study of FLIM in the frequency domain for latent fingerprint detection for suspect identification (Seah *et al.*, 2005).

In this paper, we further demonstrate the capacity of TRFM as a practical analytical tool in the forensic sciences through a comprehensive study of the observed emission from gunshot residue (GSR). There has long been a point of conjecture in various literatures concerning the origin of this emission (Lewis *et al.*, 2005). Here, we present for, what is to our knowledge the first time, high-resolution spatially and temporally resolved images of GSR particles obtained via

TRFM. We specifically address this known point of conjecture and show that by measuring the emission in the time domain, the recorded signal is in fact a result due to both fluorescence and light scattering processes.

2. Gunshot residues in forensic science

In criminal cases in which one or several weapons are involved, it is important to investigate the traces of gunshot left on the victim and/or the shooter to clarify the background of the case in question. Traces that remain on the victim include bullet holes (which occur when a bullet or shot penetrates an article of clothing), gunshot wounds to tissues and/or bone, and GSR in and around the area of the entrance hole or wound. GSR is a particularly useful piece of forensic evidence that can assist with reconstruction of the crime. Not only can it be used to identify a particular bullet hole in a material, it may also yield useful information as to firing distance, identification of a suspect as having recently used a firearm and (in some circumstances) help distinguish suicide from suspicious death (Ross, 1993).

The formation of GSR arises from the cooling and condensation of the gases produced by the combustion reactions within the firearm: predominately water vapour and carbon dioxide. Most of the gases are expelled down the barrel of the weapon, however significant quantities escape from the many openings present within the weapon such as the breech, ejection ports and the trigger. As the gases cool and condense, they form particles that are referred to collectively as GSR. The residues consists of a variety of materials and may be associated with particles of the projectile or the projectile's jacket, unburnt particles of smokeless powder, partially burnt particles of powder, combustion products, lubricants and particles of primer residue.

A number of methods based on bulk analysis have been employed throughout recent history in order to identify GSR. Wet chemical tests (Harrison and Gilroy, 1959), neutron activation analysis (Ruch *et al.*, 1964), atomic absorption spectrophotometry (Wolten *et al.*, 1979), anodic stripping voltammetry (Bratin, 1981) and scanning electron microscopy (Boehm, 1971) are among the most common. To date, most of these procedures have concentrated on the inorganic fraction of GSR and, in particular, elemental analyses targeting lead, barium and antimony have been widely used since it is this elemental combination that is characteristic of nearly all GSR (Thornton, 1994). However, one of the largest limitations of this destructive elemental analysis is that it cannot be discounted that the elements were picked up separately from the surrounding environment. Particles containing lead and bromine are found in a variety of everyday products; the emissions from the combustion of leaded petrol, in plumbing materials, battery plates, solder, glass and paint. Similarly, barium is found in paint and in automobile grease and barium sulphate from paper is likely the dominant source of environmental barium found on the hands (Andrasko and Maehly, 1977). To exemplify this point, Havekost and co-workers studied the distribution of barium on the hands of 269 non-shooters and found a statistically significant increased level of Ba and Sb on the hands of subjects who were employed as automobile mechanics, electricians and construction workers (Havekost *et al.*, 1990).

With the clear need for an alternative technique that can be used to unambiguously identify GSR for precise forensic evidence, a number of studies followed using optical spectroscopic methods in an attempt to provide a qualitative determination of GSR (Ross, 1993; Rowe, 2000; Romolo and Margot, 2001). Using forensic light sources (e.g. Polilight® and Omnichrome® 9000) for incident illumination in conjunction with filter goggles these studies have revealed a number of interesting findings, however, general acceptance as to the origins of the source of contrast [be it luminescence (e.g. fluorescence) or light scattering] is still lacking. For example, visualization of powder patterns, revealing 'fluorescence' of partially burnt nitrocellulose particles following illumination with 415-nm light, has been reported (Rowe, 2000) and 'photoluminescence' from burnt or semi-burnt propellant particles has also been observed (Lennard and Stoilovic, 2004). Weak orange 'fluorescence' (574–600 nm) from smokeless GSR particles has also been reported (Ross, 1993), and Elworthy successfully matched excitation and 'emission' spectra of unknown GSR with that in a known library to identify a specific ammunition type (Elworthy, 2002).

Considering the various points of conjecture concerning the origin of the observed emission from GSR under a variety of illumination conditions, it is our working hypothesis that: (a) studying the emission in the time domain has enormous potential in this context by (at the very least) providing some insight into which (if any) photoluminescence process is occurring and (b) by exploiting endogenous sources of contrast from within GSR particles, the usefulness of FLIM as a highly sensitive and specific forensic tool will be demonstrated.

3. Materials and methods

3.1. Sample preparation

Partially burnt propellant particles (GSR's) were collected from Winchester Super X 125 grain Jacketed Hollow Point .38 special ammunition (Batch number: BFB50-93049, Winchester Ammunition, East Alton, Illinois) fired from a .38 calibre revolver (Smith & Wesson, Springfield, Massachusetts). The firearm was discharged at a target consisting of calico (cotton) material mounted on a cardboard backing frame at a firing distance of approximately 60 cm (measured as the end of the firearm barrel to target). Figure 1 shows the appearance of the bullet hole and distribution of expelled GSR particles under (a) ambient light and (b) a forensic light source, respectively. For imaging, eight samples (partially burnt propellant particles)

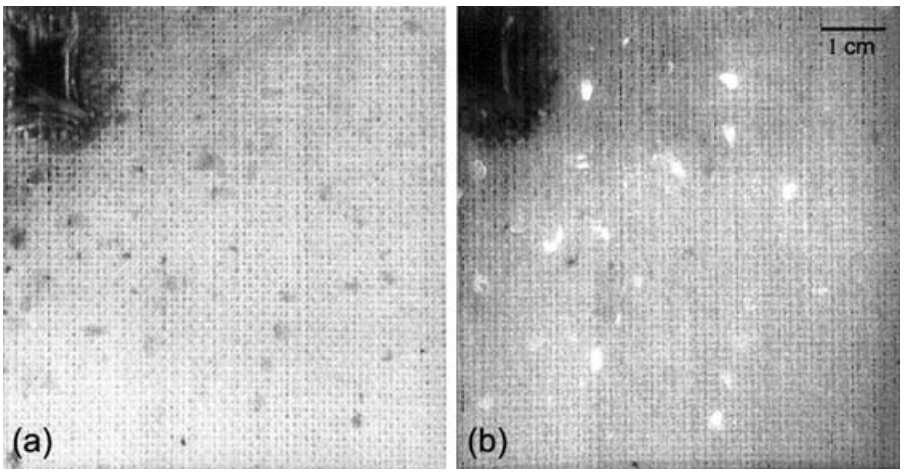

Fig. 1. Distribution of discharged gunshot residues on a target from a firing distance of 60 cm as observed under (a) ambient light and (b) a forensic light source.

were removed and individually mounted on glass microscope slides, then sealed under a 0.17-mm cover slip suitable for confocal microscopy.

3.2. Time-resolved confocal laser scanning microscopy

A schematic diagram of the instrument used in our imaging experiments is given in Fig. 2. Individual GSR particles were excited with a 400 nm ultrashort-pulsed laser beam ($\tau_p \sim$ 200 fs) produced from the frequency doubled output of a Ti : Sapphire laser (Coherent, Mira, Santa Clara, CA, USA) tuned to 800 nm and operating at a repetition rate of 76 MHz. The illumination was delivered to the sample mounted in an inverted microscope (IX-71, Olympus, Center Valley, PA, USA) through a scanning unit (Olympus FV-300) containing x and y galvanometer scan mirrors and via a transfer lens, L producing a focused scanning spot moving across the nominal back aperture of an imaging objective, O (Nikon, 60× 1.4 NA, oil, Melville, NY, USA). The de-scanned signal from the sample was filtered, D_1 (450-DCLP, Omega Optical, Inc., Brattleboro, VT, USA) and reflected by a mirror, M_1 through a confocal pinhole, P (200 μm) before impinging on an enhanced silver mirror, M_2 mounted at 45° housed in a custom made turret designed to slide into the standard filter block mount of the FV-300 scan unit. This mirror reflects the collected photons onto a peltier-cooled fast photomultiplier tube (PMC-100-1, Becker & Hickl, Berlin, Germany), which is masked with a blocking filter, BF and mounted on an x-y translation stage that aids in optimizing the signal level. Alternatively, the fluorescence signal may be directed to an additional side port on the IX-71 microscope by inserting a dichroic mirror, D_2 into the beam path (shown greyed in Fig. 2) where micro-spectroscopy with a high-resolution (0.09 nm) imaging spectrograph (Jobin Yvon, Triax 550, Edison, NJ, USA) equipped with a liquid-nitrogen cooled CCD (Jobin Yvon, SpectrumOne) can be performed.

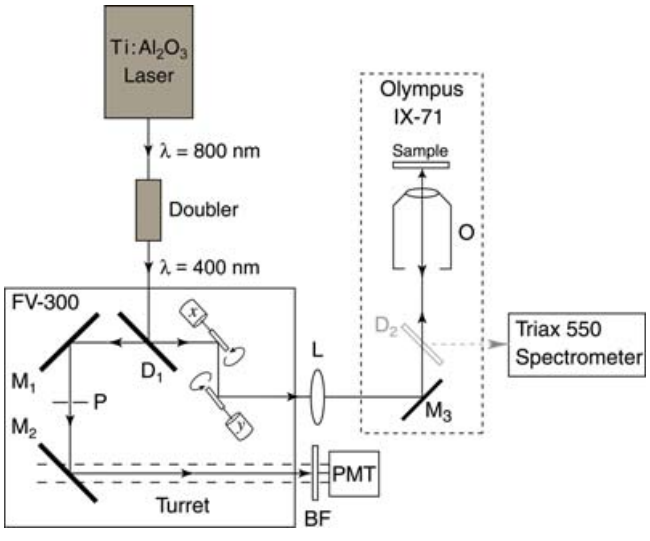

Fig. 2. Schematic diagram of the time-resolved scanning confocal fluorescence microscope. M_1, M_2, M_3: Mirrors, D_1, D_2: Dichroic Mirrors, P: Pinhole, L: Transfer Lens, O: Imaging Objective and BF: Blocking Filter.

Time-resolved imaging was carried out by time-correlated single photon counting (TCSPC) (O'Connor and Phillips, 1984) using a complete electronic system for recording fast light signals (SPC-830, Becker & Hickl). Two dimensional fluorescence images were collected by synchronizing photon counts (anode pulses from the photomultiplier tube) with the x and y laser scanning signals of the microscope. Laser pulses are detected by directing a small fraction of the output beam of the Ti : Sapphire laser onto an external high-speed photodiode module (PD-400, Becker & Hickl) and these pulses are used to determine the detection time of a photon (an anode pulse from the photomultiplier tube) relative to a laser pulse. Timing starts on receipt of a detected photon and stops after the measured

time lapse to the next laser pulse. The temporal evolution of the emission probability after excitation is described by a histogram of these time spans whereby each counting event is allocated to a temporal bin for each pixel of the image (Becker *et al.*, 2004). Image reconstruction is accomplished by an off-line commercial software package (SPCImage, Becker & Hickl) that fits the experimentally determined fluorescence decay at each pixel (with the basic assumption that the fluorescence decay histogram for each pixel is well described by either a single or multi-exponential decay) by a function which is the convolution of the instrument response function and a decay model of the form:

$$I(t) = \sum_{i=0}^{n} a_i \exp(-t/\tau_i) + c, \qquad (1)$$

where $I(t)$ is the fluorescence intensity at time t after the excitation pulse, n is the total number of decaying species in the exponential sum and c is a constant pertaining to the level of background light present in most practical situations. The parameters τ_i and a_i are the fluorescence lifetime and fractional contribution of the ith emitting species, respectively. The final values are arrived at by a process of iterative re-convolution (through the minimization of the deviation between the experimental and calculated decay profiles: χ^2) using the convolved function and a routine for non-linear curve fitting (Levenburg–Marquardt). These data are displayed as a pseudo-coloured image with colour representing lifetime (Bergmann, 2003).

4. Results

4.1. Micro-spectroscopy

Preliminary studies were conducted on individual GSR particles using a fluorescence spectrophotometer (Hitachi F-4010, Tokyo, Japan) with the aim of obtaining excitation and emission spectra that could be used to select the optimum laser excitation wavelength and optical filters required for efficient detection of any fluorescence signal. The GSR sample was mounted in the solid substrate holder and excitation and emission spectra were collected over the wavelengths in the range of approximately 220–730 nm. However, after examining multiple samples of GSR we were not able to detect any emission from the particles across the entire excitation range available. This suggests (in the first instance) that the previously observed phenomenon from GSR under forensic light sources is likely due to a scattering rather than an absorption–emission process.

In order to investigate further, we performed micro-spectroscopic analysis on an individual GSR particle by operating the confocal laser scanning microscope in the alternative detection mode; whereby emission from the sample is directed to the imaging spectrograph (Fig. 2). A point scan was performed at a focal plane approximately 5 μm into the sample and the recorded emission spectrum is given in Fig. 3. The spectrum reveals a relatively broad emission band (approximately 120 nm at full width half maximum) centred at approximately 600 nm, which is consistent with earlier reports of weak orange fluorescence (574–600 nm) from smokeless GSR particles (Ross, 1993). This result clearly suggests that the observed emission from GSR particles is likely the result of an absorption–emission process, that is, fluorescence; however, the lack of structure in the spectrum suggests the presence of multiple emitting species. It should be pointed out that there are fundamental differences between the spectrophotometer instrumentation and that used in the micro-spectroscopic investigation of GSR that may account for this difference in observation. Compared with tight focusing (down to a few micrometres) of 400 nm high-energy pulses ($\sim$ 0.5 nJ) by the imaging objective, the illumination provided by the spectrophotometer is sourced from a 150 W xenon lamp and is used to expose the entire sample simultaneously (i.e. no focusing). This extreme difference in power density will clearly affect the probability of photon absorption and, therefore, fluorescence emission. Furthermore, since the configuration of the fluorescence spectrophotometer is such that incident light is evenly dispersed across the sample it is extremely unlikely that fluorophores residing at greater depths in the sample will be excited.

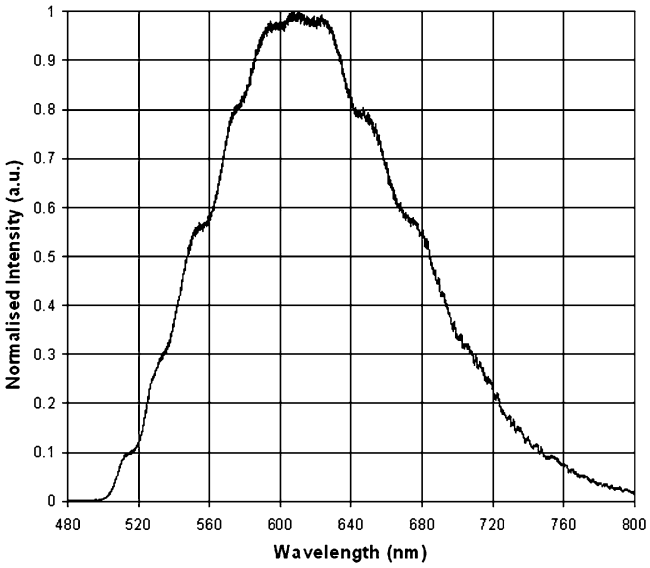

Fig. 3. Recorded emission spectrum from an individual GSR particle. The sample was point scanned at an axial depth of approximately 5 μm into the particle with 400 nm pulsed excitation.

4.2. Time-resolved Imaging

In order to confirm the mechanism of the previously observed emission from GSR's using micro-spectroscopic techniques we conducted preliminary time-resolved imaging studies on eight individual GSR particles. The ability to examine and

analyse individual particles at high spatial resolution provides far more information than using methods of bulk analysis (see Section 2.1) since primer and bullet related residues often have characteristic morphologies that reflect the mode of formation and their compositions vary considerably (Romolo and Margot, 2001). Furthermore, by observing the emission properties in the time domain, simple differentiation of an excited state fluorescence lifetime from instantaneous scattered light (or other luminescent processes) from a sample can be achieved by examining photon detection times relative to an input laser pulse.

The results are given in Figs 4(a) and 4(b) (best viewed in colour), which show two representative confocal time-resolved images obtained from a single GSR particle. The resulting images are reconstructed by summing the individual photon counts in each time channel at each pixel to obtain intensity and the process of false colour mapping is described in Section 3. The total acquisition time per image set (which comprises 256×256 pixels) was 90 s at average photon count rate of approximately 0.4 MHz. In each case, attenuation of the optical signal was required in order to reduce the photon count rate at the detector to within a suitable range for the SPC830 TCSPC electronics (approximately 0.5–1.0 MHz). In this range, longer acquisition times are required in order to obtain a sufficient number of photons for each of the histogram distributions at each pixel to ensure accurate two-exponential curve fitting.

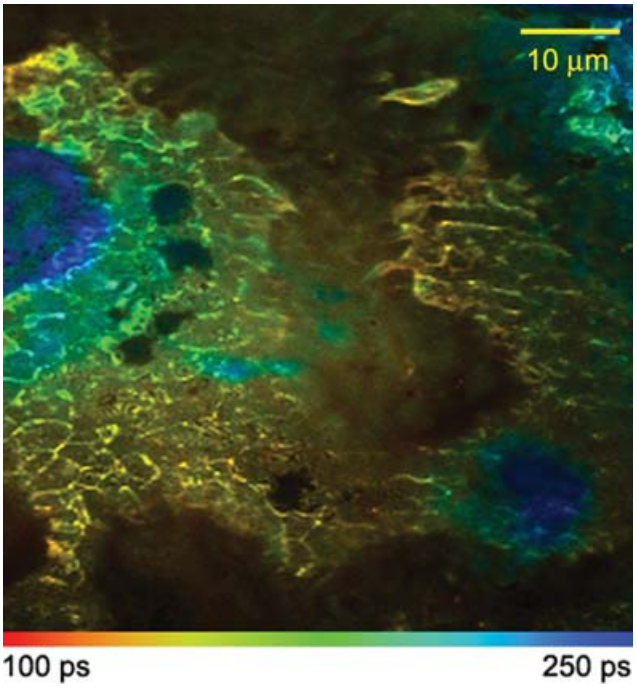

Fig. 4(a). Representative confocal time-resolved image of a single GSR particle close to the surface of the sample. The image is almost entirely a result of the dominant ($a_1 \sim 96\%$) short time component, τ_1, mapped between 100 ps and 250 ps red-to-blue, which is likely due to scattered excitation and a variety of short-lived emitting species.

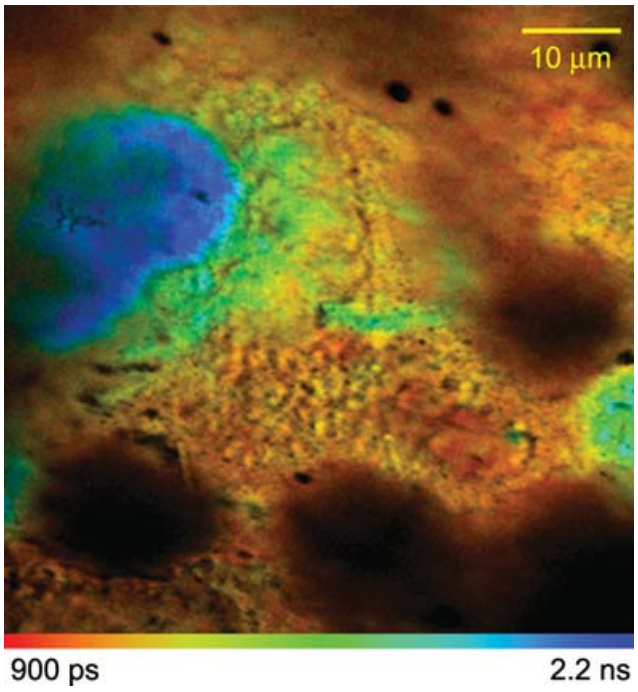

Fig. 4(b). Representative confocal time-resolved image of a single GSR particle recorded 5 μm into the sample relative to Fig. 4(a). The sub-dominant ($a_2 \sim 26\%$) fluorescence component is mapped between 0.9 ns and 2.2 ns red-to-blue, which clearly highlights the spatial variation of the excited state lifetime of the emitting species throughout the particle.

A comparison of the images reveals distinct differences in the temporal and spatial distribution of the emitting species, which is likely due to a number of factors including differences in the local microenvironment (both chemical and physical). The time-resolved image given in Fig. 4(a) was acquired from a focal plane close the surface of the particle and is the result of a two-exponential model fit. Analysis reveals that the image is dominated almost entirely ($a_1 \sim 96\%$) by an extremely short time component τ_1, which has been colour mapped over the range of 100 ps to 250 ps (red-to-blue). Given that these time scales are of the order of the measured instrument temporal response of the optical system (approximately 230 ps), we attribute the origin of this signal in part to scattering of the incident illumination (i.e. the lower end of the measured range). However, considering that convolution has been used in the fitting procedure (allowing fast processes of the order of approximately 50 ps to be resolved) the measured lifetime values at the upper end of this range are clearly too large to be attributed to scattered light alone, and are more suggestive of the presence of a variety of short-lived fluorescent species throughout the sample. This is further exemplified if one considers the spatial variation of the lifetime of this short decay across the entire image, which would not be expected if the measured signal was entirely due to scattered excitation.

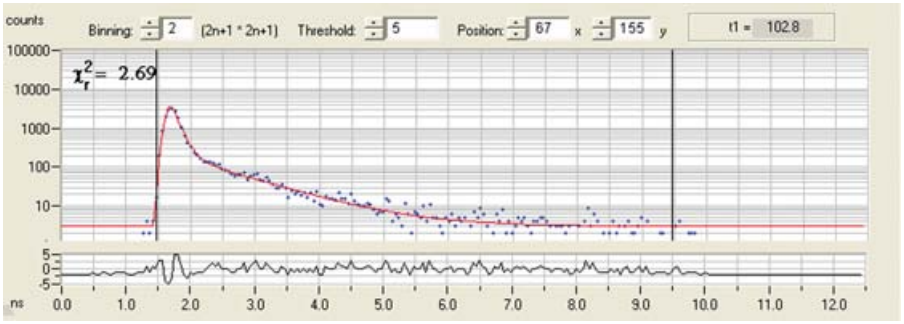

Fig. 5. Recorded photon-count histogram at pixel (67 155) in the time-resolved image of Fig. 4(a). The two-exponential decay model fit reveals a dominant short component ($\tau_1 \sim 0.1$ ns), and a sub-dominant ($a_2 \sim 4\%$) long component ($\tau_2 \sim 1.0$ ns).

Figure 5 shows the measured decay histogram from a representative pixel (67,155) of the time-resolved image shown in Fig. 4(a). Observation of Fig. 5 clearly reveals a dominant short component in the decay, however, there is also clear evidence of a (or possibly a distribution of) longer-lived emitting species ($\tau_2 \sim 1.0$ ns), albeit a small fractional component ($a_2 \sim 4\%$). In order to investigate this feature further Fig. 4(b) was acquired from the same transverse coordinates on the GSR particle but at an axial depth approximately 5 μm deeper into the sample (relative to Fig. 4a). A two-exponential model decay function was again implemented that yielded accurate fitting of the data that forms the basis of the time-resolved image. By contrast to Fig. 4(a), Fig. 4(b) exhibits a significant component in the exponential sum ($a_2 \sim 26\%$) of a longer-lived emitting species, τ_2, which is mapped between 0.9 ns and 2.2 ns, red-to-blue. For comparison to Fig. 5, the measured decay histogram from the same representative pixel (67 155) has been taken from the time-resolved image of Fig. 4(b) and is given in Fig. 6 (i.e. the same transverse spatial location but now from the deeper axial section). Given the obvious decay profile and the associated time scale, this result is clearly indicative of fluorescence and was confirmed by independently imaging all 8 samples of GSR particles formed from the same ammunition/firearm type.

It should be pointed out that there is still likely a significant degree of scatter and the possibility of a number of short-lived fluorescence processes contributing to the recorded decay function at each pixel in Fig. 4(b), and that the fluorescence emission is highly spatially localized (in all three dimensions). Minimal adjustment of the microscope's translation stage drastically reduces the fluorescence photon count rate to a few tens of kHz at some spatial locales. This result is somewhat expected and can be understood if one considers the complexity and inhomogeneous formation of individual GSR particles, which is addressed in the discussion below.

5. Discussion

The results presented in Sections 4.1 and 4.2 are particularly encouraging in the context of forensic applications since they clearly demonstrate the feasibility of a new non-destructive method of imaging individual GSR particles, and further, offer a potential method to unambiguously identify the origin of such particles (i.e. from a particular firearm and/or ammunition combination) without the need for extensive sample preparation. However, determination of the exact source of the fluorescence emission is difficult to allude to, primarily due to the molecular complexity of the resultant

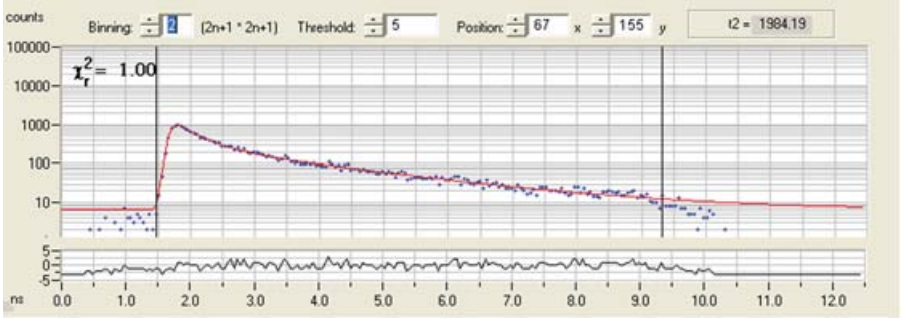

Fig. 6. Recorded photon-count histogram at pixel (67 155) in the time-resolved image of Fig. 4(b). By contrast to Fig. 5, the two-exponential decay model fit exhibits a significant contribution ($a_2 \sim 26\%$) from a longer-lived emitting species (average $\tau_2 \sim 1.6$ ns) in the exponential sum, which is clearly indicative of fluorescence.

GSR particle and the arduous conditions under which it is formed.

Smokeless propellants are based on nitrocellulose, which is produced by the nitration of cotton linters using a mixture of nitric and sulphuric acids. These types of propellant can be classified as either being single base (with nitrocellulose as the sole propellant), double base (containing nitrocellulose and nitroglycerine), or triple base (double-base that also contains nitroguanidine). Though it is unlikely that any of the nitro-compounds present in the ammunition casing would be inherently fluorescent, the presence of various surface coatings and propellant additives (such as stabilizers, oxidizers and plasticizers) give rise to the possibility of the formation of a plethora of GSR particles containing molecular species that may well be. So too do other factors in addition to the chemical composition that influence the rate at which the propellant burns. Single- and double-base propellant grains can have various physical geometries including long or short tubes, rods, rings, cubes, disks or flakes (to name but a few) that will dictate to some extent the final properties of the newly formed GSR particle.

Considering this level of complexity and variability, it should be pointed out the results presented in this study are by no means an attempt at assigning *specific* fluorescence lifetimes to any particular emitting species (be it known or not) at every spatial locale of a given specimen (i.e. at every individual pixel of the image), which are then to be compared on a pixel-by-pixel basis with images of different particles. In all actuality, analytical methods of this kind would likely prove rather ineffective for positive identification of individual GSR particles that have been discharged from different firearm and/or ammunition combinations. Rather, what the data presented in this paper clearly highlights is the fact that resolving the signal in the time-domain does allow for spatial differentiation of the magnitude of a *distribution* of lifetimes, which would likely prove to be a more effective method of positive identification of the rather unique GSR particles. This is somewhat exemplified by the fact that in all eight imaging cases of GSR particles formed from the same ammunition/firearm type, the distribution of the longer-lived emitting species was consistently more spatially localized deeper (approximately 3–6 μm) into the sample/particle. As a further example, it can be seen from inspection of Fig. 4(b) that the distribution of the long-lived emitting species is particularly aggregated in certain transverse regions of the image plane, which appear as well defined blue circles in Fig. 4b).

6. Conclusion

We have applied TRFM to imaging studies of individual GSR particles ejected from a .38 calibre revolver fired at a calico material target at a distance of 60 cm. It is demonstrated that when illuminated with 400 nm nanojoule optical pulses from an ultrashort-pulsed laser, fluorescence emission is observed from a variety of unidentified fluorescent molecules. Studying this emission in the time-domain reveals a distribution of two-component exponential decays, which is dominated by a 100–250 ps short-time component. This is indicative of a high degree of scattering of the incident illumination and a variety of short-lived emitting species. The fluorophore lifetimes of the longer-lived emitting species were found to range between approximately 0.9 and 2.2 ns, depending on the spatial position throughout the sample. This is expected since the excited state lifetime is particularly sensitive to the local microenvironment.

We have clarified a long-standing point of conjecture when visualizing GSR particles using forensic light sources; the observed emission is a combination of fluorescence and a light scattering process. At the current time the time-resolved method for detecting GSR has not been fully optimized, however, its potential for use as a forensic screening method is clear. We expect the results of this study to act as a precursor to future work that may extend this technique to examination of GSR particles from a variety of different ammunition types and/or firearms.

Acknowledgements

The authors wish to thank Mr. P. Ross of the Victoria Police Forensic Services Laboratory for providing the GSR samples. At the time this research was undertaken, Dr. D. Bird was supported by the Victorian Institute of Chemical Sciences (VICS).

References

Andrasko, J. & Maehly, A.C. (1977) Detection of gunshot residue on the hands by scanning electron microscopy. *J. Forensic Sci.* **22**, 279–287.

Bastiaens, P.I. & Squire, A. (1999) Fluorescence lifetime imaging microscopy: spatial resolution of biochemical processes in the cell. *Trends Cell Biol.* **9**, 48–52.

Becker, W., Bergmann, A. & Weiss, G. (2002) Lifetime imaging with the Zeiss LSM-510. *Proc. SPIE*. **4620**, 30–35.

Becker, W., Bergmann, A., Hink, M.A., Konig, K., Benndorf, K. & Biskup, C. (2004) Fluorescence lifetime imaging by time-correlated single-photon counting. *Microscopy Res. Tech.* **63**, 58–66.

Bergmann, A. (2003) Data Analysis Software for Fluorescence Lifetime Imaging Microscopy. Becker & Hickl GmbH, Berlin.

Bird, D.K., Eliceiri, K.W., Fan, C.-H. & White, J.G. (2004) Simultaneous two-photon spectral and lifetime fluorescence microscopy. *Appl. Opt.* **43**, 5173–5182.

Bird, D.K., Yan, L., Vrotsos, K., Eliceiri, K.W., Vaughan, E.M., Keely, P.J., White, G. & Ramanujam, N. (2005) Metabolic mapping of MCF10A human breast cells via multiphoton fluorescence lifetime imaging of the coenzyme NADH. *Cancer Res.* **65**, 8766–8773.

Boehm, E. (1971) Application of the SEM in forensic medicine. *Scanning Electron. Microsc.* **62**, 553–560.

Bratin, K. (1981) Determination of nitro aromatic, nitramine, and nitrate ester explosive compounds in explosive mixtures and gunshot residue by liquid chromatography and reductive electrochemical detection. *Anal. Chimica Acta*. **130**, 295–311.

Cubeddu, R., Pifferi, A., Taroni, P., Torricelli, A., Valentini, G. & Sorbellini, E. (1999) Fluorescence lifetime imaging: an application to the detection of skin tumors. *IEEE J. Sel. Top. Quantum Electron.* **5**, 923–929.

Dickinson, M.E., Simbuerger, E., Zimmerman, B., Waters, C.W. & Fraser, S.E. (2003) Multiphoton excitation spectra in biological samples. *J. Biomed. Opt.* **8**, 329–338.

Dowling, K., Dayel, M.J., Lever, M.J., French, P.M.W., Hares, J.D. & Dymoke-Bradshaw, A.K.L. (1998) Fluorescence lifetime imaging with picosecond resolution for biomedical applications. *Opt. Lett.* **23**, 810–812.

Eliceiri, K.W., Fan, C.-H., Lyons, G.E. & White, J.G. (2003) Analysis of histology specimens using lifetime multiphoton microscopy. *J. Biomed. Opt.* **8**, 376–380.

Elworthy, I. (2002) Detection of gunshot residues using the polilight. *16th International Symposium on the Forensic Sciences*. National Convention Centre, Canberra, ACT, Australia.

Harrison, H.C. & Gilroy, R. (1959) Fire arms discharge residues. *J. Forensic Sci.* **4**, 184–199.

Havekost, D.G., Peters, C.A. & Koons, R.D. (1990) Barium and antimony distributions on the hands of non-shooters. *J. Forensic Sci.* **35**, 1096–1114.

Lakowicz, J.R. (1999) *Principles of fluorescence spectroscopy*, 2nd ed. Kluwer Academic/Plenum Publishers, New York.

Lennard, C. & Stoilovic, M. (2004) The practice of crime scene investigation. *Application of Forensic Light Sources at the Crime Scene* (ed. by J. Horswell), CRC Press, Boca Raton, FL.

Lewis, S.W., Agg, K.M., Gutowski, S.J. & Ross, P. (2005) Forensic sciences: gunshot residue. *Encyclopedia of Analytical Science*, 2nd edn. (ed. by P. J. Worsfold, A. Townshend and C. F. Poole), pp. 430–436, Elsevier, London.

O'Connor, D.V. & Phillips, D. (1984) *Time Correlated Single Photon Counting*. Academic Press, London.

Periasamy, A. (2001) *Methods in Cellular Imaging*. Oxford University Press, New York.

Romolo, F.S. & Margot, P. (2001) Identification of gunshot residue: a critical review. *Forensics Sci. Int.* **119**, 195–211.

Ross, P. (1993) Firearm discharge residues. *Expert Evidence* (ed. by I. Freckelton and H. Selby) **4**, pp. 3531–3743. The Law Book Company, Sydney.

Rowe, W.F. (2000) Firearms: residues. *Encyclopedia of Forensic Sciences* (ed. by J.A. Siegel) **2**, pp. 953–961. Academic Press, San Diego.

Ruch, R.R., Buchanan, J.D., Guin, V.P., Bellanca, S.C. & Pinker, R.H. (1964) Neutron activation analysis in scientific crime detection. *J. Forensic Sci.* **9**, 119–132.

Saitoh, N. & Takeuchi, S. (2005) Fluorescence imaging of petroleum accelerants by time-resolved spectroscopy with a pulsed Nd-YAG laser. *Forensic Sci. Int.* **152**, 249–257.

Seah, L.K., Dinish, U.S. Phang, W.F., Chao, Z.X. & Murukeshan, V.M. (2005) Fluorescence optimisation and lifetime studies of fingerprints treated with magnetic powders. *Forensic Sci. Int.* **152**, 249–257.

Thornton, J.I. (1994) The chemistry of death by gunshot. *Analytica Chimica Acta.* **288**, 71–81.

Toniolo, L., Sansonetti, A., Colombo, C., Cubeddu, R., Valentini, G. & Comelli, D. (2004) Fluorescence Lifetime Imaging. *Exploring David: Diagnostic Tests and State of Conservation* (ed. by S. Bracci, F. Falletti, M. Matteini and R. Scopigno), pp. 154–160. Giunti Editore, Florence-Milan, Italy.

Wagnieres, G.A., Star, W.M. & Wilson, B.C. (1998) In vivo fluorescence spectroscopy and imaging for oncological applications. *Photochem. Photobiol.* **68**, 603–632.

Wang, X.F., Periasamy, A., Herman, B. & Coleman, D.M. (1992) Fluorescence lifetime imaging microscopy (FLIM): instrumentation and applications. *Crit. Rev. Anal. Chem.* **23**, 365–369.

Wolten, G.M., Nesbitt, R.S. & Calloway, A.R. (1979) Particle analysis for the detection of gunshot residue. II. Occupational and environmental particles. *J. Forensic Sci.* **24**, 423–430.

